Structural and transport properties of Fe/Ti multilayers

1990 J. Phys.: Condens. Matter 2 95

(http://iopscience.iop.org/0953-8984/2/1/007)

J. Phys.: Condens. Matter **2** (1990) 95–108. Printed in the UK

Structural and transport properties of Fe/Ti multilayers

B Rodmacq†, J Hillairet†, J Laugier‡ and A Chamberod†

† Groupe Métallurgie Physique, Service de Physique, Département de Recherche Fondamentale, Centre d'Etudes Nucléaires, 85X, 38041 Grenoble Cédex, France

‡ Groupe Structures, Service de Physique, Département de Recherche Fondamentale, Centre d'Etudes Nucléaires, 85X, 38041 Grenoble Cédex, France

Received 28 June 1989

Abstract. Fe/Ti metallic multilayers with an average $Fe_{33}Ti_{67}$ composition have been studied by x-ray diffraction, Mössbauer spectroscopy and electrical resistivity as a function of period. For small periods, broad diffraction peaks characteristic of a disordered, amorphous-like structure are observed, although composition modulation still exists along the growth direction. Beyond $\Lambda = 4$ nm, crystalline Ti appears with a BCC structure. It then reverts to its stable HCP form for $\Lambda = 6$ nm, with its c axis along the growth direction. At a period of 8 nm, the iron-rich layer in turn crystallises. This correlates to a sudden decrease of the electrical resistivity. The appearance of this Fe-rich BCC phase, corresponding to the onset of magnetic ordering in the Mössbauer spectra, induces a change in the texture of the titanium layer, the c axis now lying preferentially in the plane. Anomalies in both the lattice parameters and size of the crystallites occur from this period up to about 12 nm, whereas a plateau is observed for the electrical resistivity. For larger periods, the Ti content of the Fe-rich BCC phase decreases, corresponding to the further decrease of the electrical resistivity and increase of both hyperfine field and magnetic contribution in the Mössbauer spectra.

1. Introduction

In the last few years an increasing number of studies has developed concerning the structure and properties of artificially composition-modulated films [1]. Such an interest stems from their novel structural, electrical and magnetic properties induced by the reduced thickness of each elemental layer, which can be made as thin as an atomic plane [2]. The structure of the individual layers, the organisation of the interfacial region and the coherency between layers depend mainly on the multilayer period and will influence the properties of these materials and their subsequent evolution upon annealing.

This paper presents x-ray diffraction, Mössbauer spectroscopy and electrical conductivity results in Fe/Ti multilayers prepared by DC sputtering with average atomic composition $Fe_{33}Ti_{67}$. It focuses on the influence of the multilayer period Λ ($\Lambda = t_{Fe} + t_{Ti}$, where t is the thickness of the layers) on the structural, magnetic and electrical properties of the samples. A forthcoming publication will report on their evolution upon thermal treatment.

In their stable form, HCP α-Ti (structure type Mg, $a = 0.295$ nm, $c = 0.468$ nm) and BCC α-Fe (structure type W, $a = 0.2866$ nm) present a size mismatch of about 15% in atomic radius. The respective solubilities are 0.04% Fe in α-Ti and 10% Ti in α-Fe [3]. In addition to the two compounds, BCC FeTi (CsCl type) and HCP Fe_2Ti (Zn_2Mg type),

0953-8984/90/010095 + 14 $03.50

there exists a metastable BCC solid solution extending from 0% Fe (β-Ti, structure type W, $a = 0.33$ nm) to 50% Fe, which can be retained by rapid cooling [4]. On the other side of the phase diagram, the solubility of Ti in α-Fe can also be extended to about 20% Ti by quenching [5]. Finally, fast quenching at the $FeTi_2$ composition can produce a metastable FCC phase (type $NiTi_2$, $a = 1.13$ nm) or a quasicrystalline structure [6]. Amorphous Fe–Ti alloys have also been produced by sputtering in a wide composition range extending from 30% to 80% Fe [7–9]. It is thus interesting to look at Fe/Ti multilayers around the $Fe_{33}Ti_{67}$ composition since a variety of different crystallographic structures can be obtained depending on the preparation conditions.

We recently presented some x-ray diffraction and Mössbauer spectroscopy results on Fe/Ti multilayers [10] in which the thickness of the iron layer was kept constant at 1.5 nm while that of the titanium layer was varied between 0.5 and 8.9 nm. From these results we concluded that, although composition modulation could be observed whatever the thickness of the Ti layer, some mixing of Fe and Ti occurred in all the samples studied, leading to amorphous-like diffraction patterns and Mössbauer spectra for Fe and Ti layers of about the same nominal thickness. Similar conclusions were also drawn by Chason *et al* [11] from a study of the influence of the period on the structure of Fe/Ti multilayers at the average $Fe_{50}Ti_{50}$ composition.

2. Sample preparation

Fe/Ti multilayers were grown by triode DC sputtering by alternately depositing Fe and Ti layers on a water-cooled glass substrate from Fe (99.995%) and Ti (99.95%) targets. The targets being shielded from one another, alternating deposition was carried out by feeding either the Fe or Ti target, the substrate being rotated to ensure a good planar homogeneity of the thickness of the deposit. Under these conditions it was possible to obtain relatively thick samples ($\simeq 4\ \mu$m) with a planar variation of thickness (that is of period) lower than 2% over an area of about 6 cm^2. This was inferred from x-ray and electrical resistivity measurements on a series of strips 2.8 mm wide covering the whole surface of the substrate. The thickness of the layers was monitored by use of a quartz resonator calibrated with pure Fe and Ti films about 1 μm thick. Deposition rates of about 7 nm min^{-1} for Fe and 5 nm min^{-1} for Ti were used. On account of the bulk densities of iron and titanium, samples with average composition $Fe_{33}Ti_{67}$ were prepared, leading to a nominal thickness ratio of $\frac{1}{4}$ to $\frac{3}{4}$ for the Fe and Ti elemental layers respectively. The period of the multilayers was varied between about 1 to 100 nm.

Two kinds of sample were prepared, thin ones ($\simeq 800$ nm) adherent to the glass substrate and thicker ones ($\simeq 4\ \mu$m) which could be removed from the substrate for transmission experiments (x-ray diffraction or Mössbauer spectroscopy). No difference in the structure was detected between the two types of sample obtained under similar experimental conditions, except total thickness.

For the sake of comparison, other series of samples were prepared in order to study the influence of the deposition temperature (liquid N_2 instead of water as cooling agent) or the influence of the relative thickness of the Fe and Ti layers (average atomic composition of $Fe_{60}Ti_{40}$ instead of $Fe_{33}Ti_{67}$, leading to equally thick Fe and Ti layers).

The accuracy in the multilayer period and the reproducibility of the samples were further checked by small-angle x-ray diffraction. Measured and nominal values were found to agree within 2% over the whole range of periods studied.

3. Results and discussion

3.1. X-ray diffraction

X-ray diffraction is a valuable tool for the study of multilayers since it can probe different directions of the scattering vector q ($= 4\pi \sin\theta/\lambda$, where 2θ is the diffraction angle and λ is the wavelength of the radiation) with respect to the layer plane. For example, the scattering vector q lies in the layer plane in symmetric transmission geometry, thus probing the crystallographic structure and crystalline coherence in the plane. On the contrary, q is normal to the layer plane in symmetric reflection geometry, then probing the structure and coherence along the growth direction. In this latter case the diffracted intensity can be written as the product of two contributions [12, 13]:

$$I(q) \sim |F(q)|^2 \times \mathcal{L}(q)$$

where $F(q)$ is the structure factor of the bilayer and $\mathcal{L}(q)$ (the Laue function) is a summation term of the contributions of the N bilayers of period Λ. This function $\mathcal{L}(q)$ will exhibit maxima at $q_n = n \times 2\pi/\Lambda$, where the integer n is the order of the reflection. The other term $|F(q)|^2$ will exhibit maxima at $q_m = m \times 2\pi/d_i$, where d_i is the Fe or Ti lattice spacing, that is for q_m values much larger than q_n since $\Lambda \gg d_i$. As a consequence of the limited thickness of the individual layers, $|F(q)|^2$ will exhibit secondary maxima on both sides of the main Bragg reflections at q_m.

Whereas the diffracted intensity at small scattering vectors will be dominated by the contribution of $\mathcal{L}(q)$ (i.e. superlattice peaks at $q_n = n \times 2\pi/\Lambda$), its shape at large q will depend on the extent of coherency between layers. Imperfections such as fluctuations in the period [12, 13] will lead to a damping of the oscillations of $\mathcal{L}(q)$ at large q, and consequently the Bragg peaks coming from $F(q)$ will practically not be affected by this modulation. This means that, in this range of scattering vectors, the layers can be considered as incoherent with respect to one another.

Inversely, since the oscillations (secondary maxima) of $|F(q)|^2$ extend on both sides of the main Bragg peaks located at q_m, and thus in particular down to $q = 0$, the intensity of the successive maxima of $\mathcal{L}(q)$ will in turn be modulated. Some of these maxima can even be absent when $|F(q)|^2 = 0$. This will be the case for a square composition profile for example when the thicknesses of the individual layers are commensurate. As an example, if the thickness of one of the layers is one-fourth of the period, all superlattice reflections of order $n = 4 \times$ integer will be absent.

Figures 1 to 3 display the observed x-ray spectra. All the diffraction patterns presented in this paper were recorded with Co Kα radiation ($\lambda = 0.179$ nm). Figure 1(*a*) shows the small-angle part of the diffraction pattern of a Fe/Ti multilayer with period 40 nm. More than 30 superlattice peaks are visible, illustrating the good quality of these metallic multilayers. Such small-angle peaks were observed in all the samples studied down to the smallest period examined ($\Lambda = 1.1$ nm). As stated above, the position of these superlattice peaks can be used to determine the period of the multilayer with good accuracy if one takes into account the refraction effects for the radiation used [14]. In this case the position of the nth peak is related to the period through:

$$\sin^2\theta = (n\lambda/2\Lambda)^2 + 2\delta$$

where δ is the deviation from unity of the refraction index.

In addition one can see in figure 1(*a*) that the $4 \times m$ orders (4, 8, 12, 16, 20) up to $m = 5$ are practically absent, in agreement with the fact that the thickness of the iron

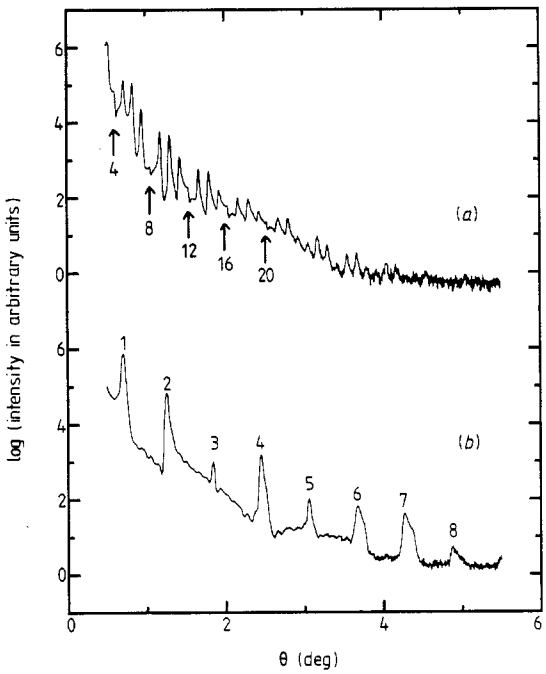

Figure 1. Small-angle superlattice peaks for Fe/Ti multilayers with (*a*) $\Lambda = 40$ nm and (*b*) $\Lambda = 8$ nm. The numbers indicate the order of the reflection.

layer is one-fourth of the period. On the contrary, one can see in figure 1(*b*) that this is not the case for smaller periods (here $\Lambda = 8$ nm). The $n = 4$ and $n = 8$ orders are no longer absent, whereas the $n = 3$ one is very weak. In the simplest model of a rectangular composition profile, this result would indicate that now the Fe layer has grown thicker than $\Lambda/4$, as a possible result of some Ti diffusion into it. We will see that this is in agreement with the large-angle results presented below.

Figure 2 presents the evolution of the large-angle diffraction patterns in reflection geometry in the region of the first Bragg peaks, whereas figure 3 shows some of the results obtained in transmission geometry in a larger angular range. In every figure the diffracted intensities are given in normalised arbitrary units.

For small periods (figures 2(*a*) and 3(*a*), $\Lambda = 2$ nm), both transmission and reflection spectra are very similar, with a broad peak around $\theta = 24°$. Both the similarity between spectra and the weak scattered intensity indicate that the scattering is isotropic in this range of periods, and that the Fe and Ti layers are mixed to quite a large extent, leading to an amorphous-like structure (the positions of the main peak and of a second one around 43° in figure 3(*a*) are close to the first two diffraction peaks of the homogeneous $Fe_{33}Ti_{67}$ amorphous alloy). Nevertheless such an amorphous phase is not homogeneous along the growth direction since superlattice peaks are present.

As Λ increases, the reflection and transmission spectra are no longer identical, as can be seen in figures 2(*b*) and 3(*b*) for $\Lambda = 4$ nm. In reflection geometry, the broad signal is now much more intense and shifts towards smaller angle, at a position very close to that of the (0002) reflection for HCP Ti. The increase of the diffracted intensity can be attributed to texture effects. In transmission geometry, the main peak is now the superimposition of two contributions (figure 3(*b*)), with a sharp peak at about 23° on top of the broad signal identical to that observed in figure 3(*a*). However a small peak

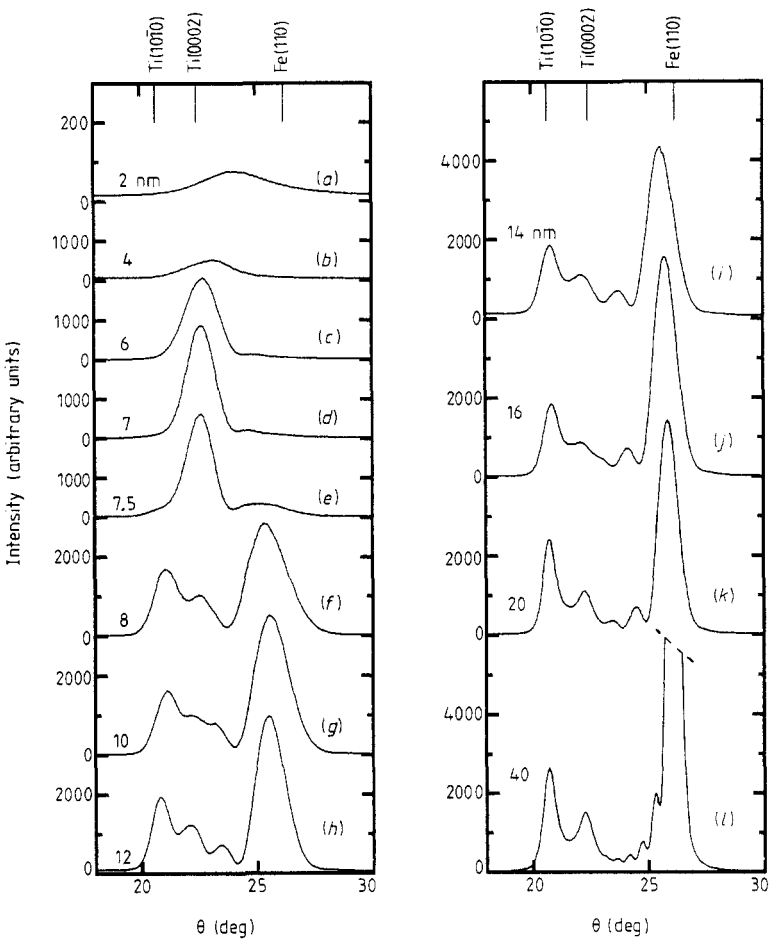

Figure 2. X-ray diffraction spectra in symmetric reflection geometry. The numbers give the value of the period. Note the enlarged intensity scale for spectrum (*a*).

also appears at about 34°. Such a peak cannot be indexed as a HCP reflection, but rather as the (200) reflection of BCC β-Ti. Since the position of the (0002) reflection for HCP Ti and of the (110) one for BCC Ti almost coincide, both structures will give the same diffraction pattern in reflection geometry in the case of textured samples. It is pointed out that cubic Ti has already been identified in Nb/Ti multilayers with small periods [15].

For $\Lambda = 6$ nm (figure 3(*c*)), a supplementary peak appears at about 20.7°, whereas that at 34° characteristic of BCC Ti is less visible. This evolution corresponds to a transformation of BCC Ti into HCP Ti as the thickness of the Ti layer increases, since the peak at 207° almost coincides with the (10$\bar{1}$0) reflection of HCP Ti. Other reflections of HCP Ti can be observed in figure 3(*c*) ((11$\bar{2}$0) at $\theta = 37°$ for example). The Ti layers are thus strongly textured, the *c* axis being oriented preferentially along the growth direction (only the (0002) and (0004) reflections are observed in reflection geometry). In addition, broad peaks at about 24° and 43° are still visible in transmission geometry, indicating that part of the sample is still amorphous, but iron-enriched since pure, crystalline Ti has

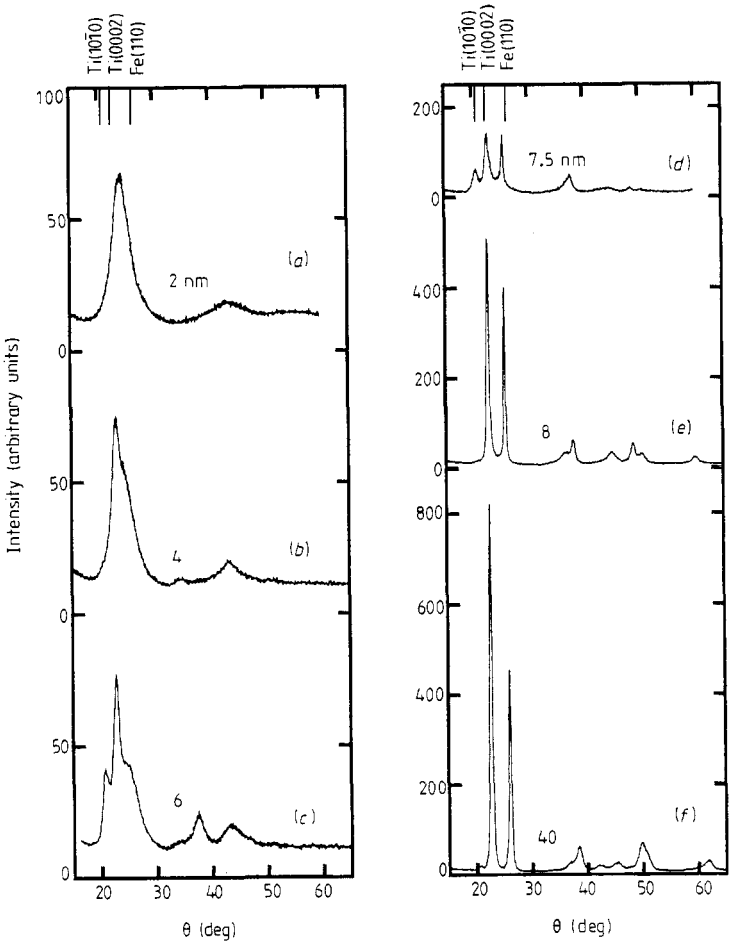

Figure 3. As figure 2 but for symmetric transmission geometry.

now appeared in the diffraction spectra. Surprisingly, the peak at 22.7° in transmission geometry is still present, despite the (0001) texture. This can be attributed to remaining BCC Ti. Finally, the small peak at about 24° in figure 2(*d*) is identified as a secondary maximum of the main reflection (as a consequence of the limited thickness of the Ti layer). From its position relative to the main peak, the thickness of the titanium layer can be estimated to lie between about 3 to 4 nm. This value is in good agreement with that derived from the width of the main peak by use of the Scherrer formula [16], and it is found to be systematically a bit smaller than the nominal thickness of the Ti layer. The fact that this secondary maximum is only observed on one side of the main peak indicates that the lattice parameter of Ti is not constant throughout the layer [17, 18]. The enhancement of the high-angle maximum compared to the low-angle one corresponds to a decrease of the lattice spacing near the interface, which could result from either some Fe diffusion into the Ti layer or distortions induced by the Fe-rich one.

As Λ reaches 8 nm (figures 2(*f*) and 3(*e*)), two important modifications occur in the diffraction spectra. The first is the appearance of an intense diffraction peak at about

25.5° both in reflection and transmission geometries (which could already be guessed in figures 2(*e*) and 3(*d*) for $\Lambda = 7.5$ nm), corresponding to the (110) reflection of a BCC Fe-rich phase. The second modification is the strong decrease of the (0002) contribution of α-Ti to the benefit of the $(10\bar{1}0)$ one at $\theta = 20.7°$ in reflection geometry. This suggests that the crystallisation of the amorphous Fe-rich layer induces a change of the texture of the Ti layer, the *c* axis being now preferentially in the plane of the layers, as shown by the transmission spectrum in figure 3(*e*) where the $(10\bar{1}0)$ reflection of α-Ti has disappeared to the benefit of the (0002) one. The Fe-rich layer is also strongly textured since only the (110) and (220) reflections are present in the diffraction pattern in reflection geometry, whereas all the reflections observed in transmission geometry correspond to ⟨110⟩ zone planes.

As was the case for Ti in the diffraction pattern of figure 2(*d*), secondary maxima of the main Fe Bragg peak can also be observed beyond $\Lambda = 8$ nm, but now they appear on the low-angle side of the main peak, indicating that the Fe lattice spacing is larger near the interface. Up to five secondary maxima can be observed in figure 2(*l*) for $\Lambda = 40$ nm. The values of the thickness of the Fe-rich layer obtained either from the width of the main peak or from the position of the secondary maxima are in very good agreement and now correspond to a layer thickness larger than the nominal pure Fe one by about 0.5 to 1 nm, whereas the thickness of the Ti layer is smaller than the nominal one, as mentioned above. Let us note that the peak at about 22.5° in figures 2(*f*) to 2(*l*) cannot be only a secondary maximum since it does not shift towards the Fe reflection as Λ increases. Its intensity is also too large (cf figure 2(*l*)). It has thus to be attributed to some remaining (0001) texture of HCP Ti, which is consistent with the existence of a small contribution of $(10\bar{1}0)$ HCP planes at $\theta = 20.7°$ in transmission geometry (figure 3(*f*)). With increasing Λ the relative contribution of this (0001) texture seems to increase slightly. The position of the (110) peak of the BCC Fe-rich phase progressively shifts towards larger angles up to the position of the (110) reflection of pure iron.

Taken together, these changes in the diffraction patterns with multilayer period can be understood by assuming that some mixing of Fe and Ti atoms takes place during the sputtering process and that the thickness of the mixed region stays the same whatever the period. Such a mixing would typically affect 1 to 1.5 nm of Fe and Ti, leading to a disordered layer with approximate thickness 2 to 3 nm. For small periods ($\Lambda < 4$ nm, that is $t_{Fe} < 1$ nm and $t_{Ti} < 3$ nm), the contribution of this mixed layer predominates, and corresponds to the broad diffraction peak in figures 2(*a*) and 3(*a*). The presence of small-angle superlattice peaks indicates that there exists a gradual composition variation throughout the bilayer. As the period is increased, the thickness of the pure Ti layer increases relative to that of the mixed layer, leading to the observed shift of the diffraction peak towards smaller angle (i.e. both the mixed layer and the pure Ti layer contribute to this peak). Crystalline Ti appears with a BCC structure in this range of periods. At a period of 6 nm, both (Fe, Ti) and Ti layers have approximately the same thickness. The Ti layer has now reverted to its stable HCP structure. It is well crystallised and textured, thus giving a more intense peak in reflection geometry than the still non-textured mixed (Fe, Ti) layer. Besides, the thickness ratio of the layers is different from $\frac{1}{4}$ to $\frac{3}{4}$, which explains why the small-angle peaks with $n = 4 \times m$ are visible. This also agrees with our recent high-resolution electron microscopy results on samples with $\Lambda = 7$ nm which show that the bilayer consists of an amorphous layer and a HCP layer with comparable thicknesses [19]. The microscopy results also confirm the existence of BCC β-Ti in this range of periods.

For larger periods ($\Lambda \geq 8$ nm, that is $t_{Fe} \geq 2$ nm), iron is then available in excess to the amount included in the mixed (Fe, Ti) layer. From the diffraction results it is inferred

that this extra iron induces both a crystallisation of the mixed layer with a (110) texture and a change of the texture of the Ti layer, the $(10\bar{1}0)$ direction now being parallel to the growth direction. Such a change occurs in a very narrow interval of periods of the order of 1 nm, corresponding to about one Fe atomic plane. Beyond $\Lambda = 8$ nm, the (110) peak of the BCC phase shifts progressively towards the position for pure iron, indicating that all the Fe atoms dissolve into this Fe-rich BCC phase, thus increasing the Fe concentration. On the contrary, this does not seem to be the case for the titanium layer, whose lattice parameters are found to be less dependent on the multilayer period, in agreement with the much smaller solubility of Fe into HCP Ti [3].

One should note that the size L of the Fe-rich crystallites in the plane of the layers (obtained from the width of the diffraction peaks in transmission geometry) goes through a maximum for periods between 8 and 20 nm, increasing first from $L = 14$ to $L = 17$ nm for $\Lambda = 10$ nm and then decreasing to $L = 10$ nm for $\Lambda = 20$ nm before increasing again slightly up to $L = 12$ nm for $\Lambda = 40$ nm. Although less marked, similar behaviour was observed for the size of the Ti crystallites. From the position of the (110) peak of the Fe-rich phase and $(10\bar{1}0)$ peak of α-Ti, it also appears that the respective lattice parameters, a, of the BCC phase and of the HCP phase are very close to each other up to periods of about 20 nm.

At still larger periods the Ti content of the Fe layers becomes negligible, and the position of the diffraction peaks tends towards that of pure BCC iron. The thickness ratio of the layers tends towards the nominal one, as shown by the absence of the $n = 4 \times m$ reflections in the small-angle region. Both $(10\bar{1}0)$ and (0001) textures are observed for HCP Ti, probably indicating that, far from the Fe layer, titanium tends to grow with the densest (0001) planes parallel to the layer plane.

For the sake of comparison, multilayered samples with the same average composition were also prepared, the substrate now being held at liquid nitrogen temperature. The x-ray scattering results show the same evolution of the structure with multilayer period as observed above, except for a larger intensity of the small-angle peaks and a less marked texture of the crystalline phases. Such a behaviour can be explained by the reduced mobility of the iron and titanium atoms (as a consequence of the lower substrate temperature), leading to both sharper interfaces and less perfect orientation of the crystallites. Nevertheless, the changes in the structure of the layers take place at the same critical thicknesses, indicating that mixing mainly occurs during the sputtering process.

In the same way, such a picture is also consistent with the results obtained on multilayers with average composition $Fe_{60}Ti_{40}$ (i.e. $t_{Fe} = t_{Ti}$). Samples with $\Lambda \leqslant 3$ nm ($t_{Fe} = t_{Ti} = 1.5$ nm) exhibit only a broad amorphous-like diffraction pattern, whereas HCP Ti and BCC Fe *simultaneously* appear for $\Lambda \geqslant 4$ nm ($t_{Fe} = t_{Ti} = 2$ nm).

3.2. Mössbauer spectroscopy

^{57}Fe Mössbauer experiments were carried out on free-standing samples 4 μm thick in transmission geometry. Such a technique probes the local environment of the iron atoms, thus enabling direct comparison with the x-ray results presented above. Figure 4 shows the evolution of the room-temperature Mössbauer spectra as a function of the period of the multilayer. The spectrum in figure 4(*a*) ($\Lambda = 2$ nm) consists of a slightly dissymmetrical doublet with a mean isomeric shift IS = 0.22 mm s^{-1} (relative to metallic iron) and mean quadrupole splitting QS = 0.34 mm s^{-1}. Both the values of the hyperfine parameters and the dissymmetry of the spectrum are similar to those observed in a

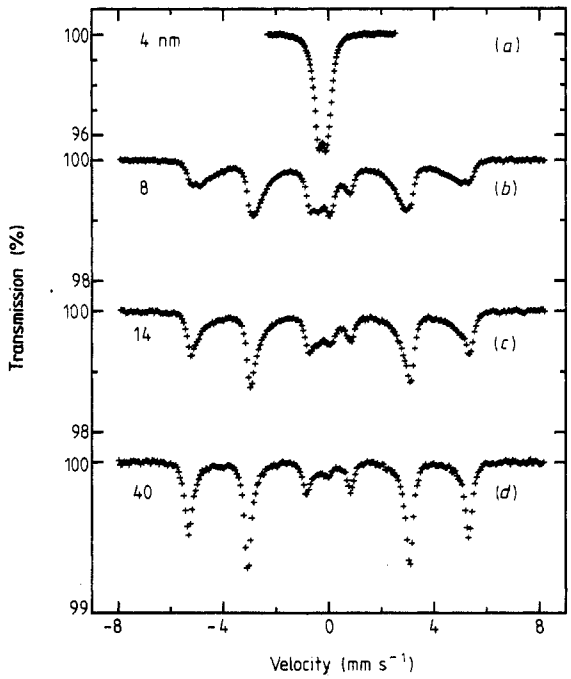

Figure 4. Evolution of the room-temperature Mössbauer spectra with period.

homogeneous $Fe_{33}Ti_{67}$ amorphous alloy [8], which confirms that, in this range of periods, the multilayer consists mainly of a mixed (Fe, Ti) disordered phase, as we concluded from the x-ray experiments. For $\Lambda = 8$ nm (figure 4(*b*)), the Mössbauer spectrum suddenly changes and a magnetic contribution appears in addition to the paramagnetic one. The six peaks of this magnetic contribution are rather broad and their position corresponds to a hyperfine field H of about 310 to 320 kOe, typical of the Fe-rich BCC phase [7]. The relative intensity of the six peaks of the magnetic contribution indicates that the magnetisation preferentially lies in the plane of the layers, as is usually observed in thin magnetic films. The width of the peaks of the magnetic contribution corresponds to a distribution in the number of nearest-neighbour iron atoms in this BCC phase since, according to the x-ray results, it contains some titanium. The magnetic spectrum will thus be the sum of contributions from iron atoms with different numbers of titanium atoms in their first coordination shell. The paramagnetic contribution can have two origins, since it can correspond either to iron atoms close to the titanium layer (and thus with a number of nearest-neighbour iron atoms smaller than that required for BCC iron to be magnetic), or to some remaining amorphous (Fe, Ti) layer at the interface.

As the period increases (figures 4(*b*) to 4(*d*)), both the width of the peaks of the magnetic spectrum and the weight of the paramagnetic contribution decrease, whereas the mean hyperfine field increases, in agreement with both a smaller Ti content of the BCC phase and a smaller relative contribution of the interfacial non-magnetic Fe atoms.

3.3. Electrical resistivity

The resistance of the as-deposited samples was measured parallel to the layers using a conventional four-probe method, with a 100 nV resolution digital voltmeter determining

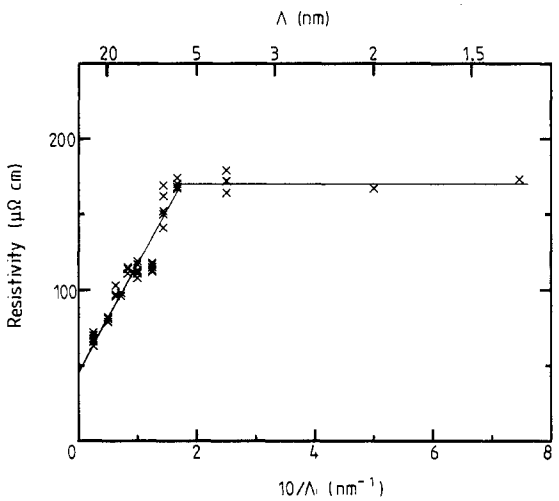

Figure 5. Variation of the room-temperature electrical resistivity with inverse period.

the voltage drop for a constant 20 mA current. The results are shown in figure 5 as a function of reciprocal bilayer thickness, Λ^{-1}, for a series of samples with average composition $Fe_{33}Ti_{67}$. The measurement temperature was 293 K. The major feature of the data is the rise of the resistivity as the period decreases. The resistivity first varies inversely with Λ from about 65 $\mu\Omega$ cm at 40 nm to about 170 $\mu\Omega$ cm at 6 nm, before it levels off at the shortest periodicities. We also prepared pure Fe and Ti films under identical sputtering conditions. The Fe films had a room-temperature resistivity of between 23 and 28 $\mu\Omega$ cm, for thicknesses going from 250 to 5 nm, compared with the usual value of 10 to 12 $\mu\Omega$ cm determined in the bulk condition. Measurements on Ti films with thicknesses between 75 and 1000 nm yielded resistivities in the interval 100 to 130 $\mu\Omega$ cm, well above the bulk reference value of 42 $\mu\Omega$ cm [20].

In a first attempt, the observed dependence of resistivity on Λ can be interpreted in the light of the conventional size-effect theory for electrons undergoing diffuse scattering at surfaces (or interfaces), originally developed by Fuchs and Sondheimer in unimetallic thin films [21, 22]. When the electronic mean-free path is comparable to the film or elemental layer thickness, the resistivity is expected to vary proportionally to the reciprocal of Λ. This is the observed trend in the Fe/Ti samples studied, at least for periods not too small (figure 5). Below about 6 nm, a saturation effect prevails since the thinnest elemental films (the Fe ones) are then only a few atomic layers thick and one is approaching the Ioffe–Regel resistivity limit, which is reached when the mean-free path becomes of the order of the interatomic spacing [23]. This overall behaviour has already been observed in a number of stratified metallic systems and appears to be inherent in these structures.

The importance of the interface effect depends on a number of parameters, such as surface roughness, eventual contamination of the interface by residual gases, possible chemical mixing and mismatch between the adjacent crystal arrays. A noticeable feature of the present system is precisely the large size mismatch of the constituent elements, which is likely to result in elastic distortions and topological disorder at the interface. On the other hand any intermixing occurring during the course of the sputtering also results in a disordered transition zone which may extend over several atomic planes.

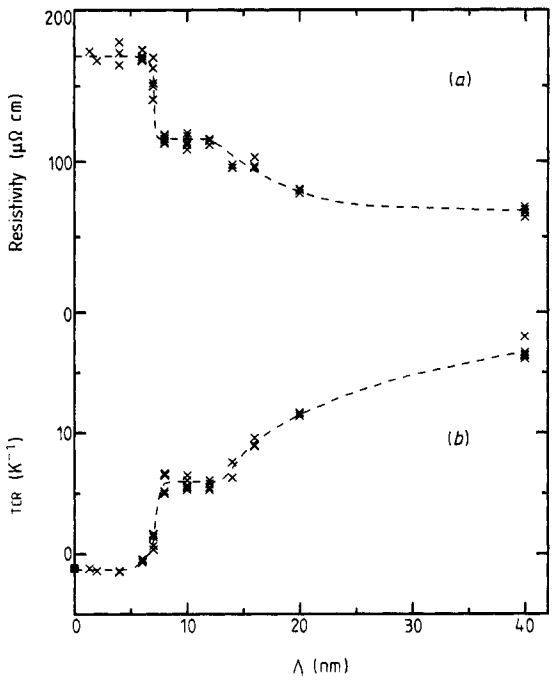

Figure 6. Plot of (*a*) the room-temperature electrical resistivity and (*b*) the temperature coefficient of resistance against multilayer period.

More importantly, like other thin films, the multilayered film structures are also subject to the grain-size effect. The grain size of the present samples has been determined by x-ray scattering (see above) to be as low as 10 to 17 nm. Thus modifications of bulk relaxation times by the grain-boundary scattering may bring a substantial contribution. In particular this is a likely explanation for the large resistivity values found in the sputtered, unimetallic Fe or Ti films. Altogether this suggests that, over a broad range of intermediate periods, the transport properties of the structures under consideration are influenced by boundary scattering, in the as-produced state. A similar view has recently been expressed to interpret resistivity effects in MoCu and MoSi stratified samples [24, 25].

Interface and grain-size effects are the most current ways of interpreting the overall dependence of resistivity on period, in multilayers. Although proper, these interpretations are often too restrictive. The reason is that they ignore the real differences which characterise the successive structural states as the period is varied. In fact deeper insight should reveal these differences. This is exemplified in figure 6(*a*). It is seen that the variation profile of resistivity with period is in reality not smooth. In contrast, it exhibits a marked structure. The salient feature is that the evolution of resistivity occurs in two distinct steps, a sudden drop between 6 and 8 nm and a progressive decrease above 12 nm, respectively, separated by an extended plateau. This structure, although detectable, was less apparent in the ρ against Λ^{-1} plot, on account of the contracted abscissa in the region of interest, in that representation.

Valuable structural information can be extracted from the results obtained. In the first place, consider the significance of the resistivity drop. It is plain that it reflects the

transition from the composition-modulated amorphous material characteristic of the shortest periods to a more ordered, stratified structure. This drastic resistivity change has indeed a striking correspondence with the advent of the iron crystallisation detected in the x-ray investigations. The appearance of iron-rich crystallites produces definite shunts for the electrical conductivity, provided that the crystallites percolate.

Next, analysis of the level of the further resistivity plateau is also informative. The finding that resistivity is not decreased below about 110 $\mu\Omega$ cm leads to the conclusion that the Fe-rich solid solution which is formed above 8 nm is still highly resistive. This high resistivity may simply be due to the high degree of disorder, topological and/or chemical, which presumably exists in this crystalline phase. The extent of the plateau is to be interpreted also in relationship to the x-ray study, which indicates that lattice coherency at the Fe-based solid solution/Ti interface is maintained until about 12 nm. This implies that the respective crystal lattices are strongly distorted, on account of the size difference between iron and titanium, thus producing displacive disorder, that is enhanced resistivity, as hinted just before. A further indication of this underlying phenomenon is brought by consideration of the grain size of the Fe-rich layers, which tends to increase for periods up to 10 nm before, contrary to expectation, it appears to decline at higher periods. This behaviour stems from the fact that elastic accommodation is made the more difficult the higher the period, that is the lower the lattice parameter of the Fe-rich strata, on account of the enriched Fe concentration. Finally, above say 12 nm, coherency no longer holds. The dominant effect is then the progressive evolution towards purer Fe strata, which explains the gradual resistivity decrease.

We turn now to the temperature coefficient of resistance (TCR). Being a differential quantity, its determination is more accurate, since all the problems linked to correcting for sample shape and dimensions drop. The TCR of about 40 samples (taken out of 20 different sputtering runs) with various bilayer thickness was determined between 253 and 293 K. The variations of this physical parameter with bilayer thickness are presented in figure 6(*b*). The detailed pattern closely resembles that of resistivity (figure 6(*a*)). Note that at the lowest periods the TCR becomes negative. It tends to a constant value identical to that for the homogeneous amorphous alloy (indicated by a full square in the figure). The negative sign of the average TCR is not specific to the metallic multilayered alloys. It has already been observed in some crystalline and a lot of amorphous alloys and metallic thin films alike. According to the Mooij rule [26], this anomaly simply denotes a transition from metallic-like behaviour to non-metallic-like behaviour in highly resistive materials. Conversely, at the highest periods. the TCR is not higher than $17 \times 10^{-4}\,K^{-1}$, which is well below the values of 65×10^{-4} and $35\text{–}55 \times 10^{-4}$ commonly found in bulk, well crystallised iron and titanium samples respectively [20, 27]. This difference is tentatively ascribed to the unusually small grain size even at the highest periods.

Finally, similar measurements performed in stratified samples too, but with composition $Fe_{60}Ti_{40}$, showed an earlier transition, starting at 4 nm. The plateau, if it exists, then looks much narrower than in the case of the $Fe_{33}Ti_{67}$ composition. These features are in satisfactory agreement with the x-ray observation that the first signs of crystallisation are manifested precisely at 4 nm, quasi-simultaneously for the Fe and Ti strata.

4. Conclusions

The various experimental approaches we followed to study the Fe/Ti multilayers lead to consistent results about the structural features and associated magnetic and transport

properties of these stratified structures. In fact, depending on bilayer thickness, four types of behaviour are distinguished.

(i) The smallest periods are characterised by composition-modulated, amorphous-like structures, as revealed by the small- and large-angle x-ray scattering experiments.

(ii) In a second class of periods, titanium is selectively crystallised, since its nominal thickness is larger than that of iron. The first signs of crystallinity appear in the diffraction pattern at a period of 4 nm. Unexpectedly enough, the observed crystalline form is then body-centred cubic. However, as soon as the period reaches 6 nm, the stable HCP structure of titanium prevails, with the *c* axis along the growth direction.

(iii) Around a critical period of 8 nm, that is a nominal Fe layer thickness of 2 nm, the iron-based layers are in turn crystallised in the form of a Fe-rich BCC phase, which brings a magnetic contribution to the Mössbauer spectra. Concomitantly the resistivity is sharply decreased. This crystallisation induces a change in texture of the Ti layers, the *c* axis now lying in the plane of the strata. The plateau in the electrical resistivity observed at larger periods coincides with rather unusual variations of the crystallite size and lattice parameter, which suggests that the elastic distortions generated by the lattice mismatch at interfaces and their accomodation play a role.

(iv) Finally, for still larger periods, the lattice parameter of the iron-rich BCC phase tends towards that for pure iron. This agrees with both the observed increase of the hyperfine field in the Mössbauer spectra and the further decrease of the electrical resistivity.

To close, it is underlined that the large size misfit between the constitutive elements and arrays confer on the Fe/Ti structures a spectrum of specific properties, including variable preferential textures, peculiar crystallisation modes and granularity, in addition to the inherent displacive disorder in the solid solutions formed. Other points of interest and further research deal with the diffusional regimes and resulting structural states which are developed upon thermal annealing.

Acknowledgments

The authors wish to thank C Mairy, J Moulin and A Pierrot for their technical assistance.

References

[1] Chang L L and Giessen B C (ed.) 1985 *Synthetic Modulated Structures* (New York: Academic)
[2] Makous J L and Falco C M 1988 *Solid State Commun.* **68** 375
[3] Murray J L 1986 *Binary Alloy Phase Diagrams* vol 2 ed. T B Massalski (Metal Park, OH: American Society for Alloys) p 1117
[4] Ray R, Giessen B C and Grant N J 1972 *Metall. Trans.* **3** 627
[5] Sumiyama K, Hashimoto Y, Yoshitake T and Nakamura Y 1983 *J. Magn. Magn. Mater.* **31–34** 1495
[6] Dong C, Hei Z K, Wang L B, Song Q H, Wu Y K and Kuo K H 1986 *Scripta Metall.* **20** 1155
[7] Liou S H and Chien C L 1984 *J. Appl. Phys.* **55** 1820
[8] Nakamura Y, Sumiyama K and Ezawa H 1986 *Hyp. Int.* **27** 361
[9] Rodmacq B, Lançon F, Chamberod A and Maret M 1988 *Mater. Sci. Engng* **97** 157
[10] Balogh J, Rodmacq B and Chamberod A 1988 *Solid State Commun.* **66** 143
[11] Chason E, Kondo H, Mizoguchi T, Cammarata R C, Spaepen F, Window B, Dunlop J B and Day R K 1986 *Mater. Res. Soc. Symp. Proc.* **58** 69
[12] Fujii Y, Ohnishi T, Ishihara T, Yamada Y, Kawaguchi K, Nakayama N and Shinjo T 1986 *J. Phys. Soc. Japan* **55** 251

[13] Clemens B M and Gay J G 1987 *Phys. Rev.* B **35** 9337
[14] Miceli P F, Neumann D A and Zabel H 1986 *Appl. Phys. Lett.* **48** 24
[15] An H and Duan F 1988 *Superlattices and Microstructures* **3** 289
[16] See, e.g., Guinier A 1964 *Théorie et Technique de la Radiocristallographie* (Paris: Dunod) p 462
[17] Majkrzak C F, Axe J D and Böni P 1985 *J. Appl. Phys.* **57** 3657
[18] Sevenhams W, Locquet J-P, Bruynseraede Y, Homma H and Schuller I K 1988 *Phys. Rev.* B **38** 4974
[19] Bourret A and Rouvière J-L *Phil. Mag.* B to be published
[20] Schröder K 1983 *Handbook of Electrical Resistivities of Binary Metallic Alloys* (Boca Raton: CRC)
[21] Fuchs K 1938 *Proc. Camb. Phil. Soc.* **34** 100
[22] Sondheimer E H 1952 *Adv. Phys.* **1** 1
[23] Ioffe A F and Regel A R 1960 *Progr. Semicond.* **4** 237
[24] Sasaki T, Kaneko T, Sakuda M and Yamamoto R 1988 *J. Phys. F: Met. Phys.* **18** L113
[25] Yamamoto R 1989 *Mat. Sci. Forum* **37** 291
[26] Mooij J H 1970 *Phys. Status Solidi* **17** 521
[27] Fisher E S and Renken C J 1964 *Phys. Rev.* A **135** 482